Interreg France (Channel Manche) England
EuroSwac
European Regional Development Fund

EUROPEAN UNION
European Regional Development Fund

Highly efficient innovative shallow-water based Sea Water Air Conditioning solution for the Channel Area

EUROSWAC

Computational Fluid Dynamic

Rev.	Status	Date	Author	Description	Checker	Approver
01	C	31/12/2022	A Bordbar, K Georgoulas	Approved	YC Lee	YC Lee

A = Issued for comments - B = Issued for approval - C = Approved

Table of contents

1. Abstract

Discharge dispersion modelling of WTEBSs can assist addressing concerns regarding their impacts on the sustainability of marine environments and provide opportunities for achieving maximum effluent mixing efficiency and understanding of the mixing behaviour of plume jets. In the present report, a new model for simulation of discharge dispersion under marine environment (i.e., combined wave and tidal flow) is developed in OpenFOAM. The model is validated against test cases for hydrodynamic modelling of different waves using analytical solution, and hydro-thermal modelling using experimental data from the literature. Then the validated model is used for modelling of discharge for 2D and 3D cases generated for providing similar conditions to available pilot SWAC system at Brixham laboratory, Brixham, UK.

2. Introduction

Discharge dispersion modelling of WTEBSs can assist addressing concerns regarding their impacts on the sustainability of marine environments and provide opportunities for achieving maximum effluent mixing efficiency and understanding of the mixing behaviour of plume jets. The application of modelling of discharge dispersion is not confined to WTEBSs as the topic is also of interest to other growing technologies such as aquafarming, desalination plants, and thermal power plants that discharge a considerable amount of wastewater directly back to waterbodies. Desalination brine, a by-product from desalination plants, comprises high concentrations of dissolved substances and suspended solids as well as possible waste heat. Thermal power plants of coastal cities discharge enormous quantities of waste heat into seas and lakes, while aquafarming effluent is typically enriched in suspended organic solids, carbon, nitrogen, and phosphorus, which may have a detrimental impact on many species living around the discharge location. In general, wastewater discharges from industrial processes are categorized into two major groups based on their density discrepancy with the ambient water bodies. If the effluent has a higher density than the ambient water, the plume of outfall discharge tends to sink, which is known as a negatively buoyant jet plume. Conversely, if the effluent has a lower density than the ambient water the effluent jet plume tends to rise, which is termed a buoyant plume. Nevertheless, the mixing behaviour of the discharged effluents can show a great diversity of flow patterns, depending on the geometric and dynamic characteristics of the environment and the discharge flow. In the present report, a new model for simulation of discharge dispersion under marine environment (i.e., combined wave and tidal flow) is developed. The model is validated against test cases for hydrodynamic modelling of different waves using analytical solution, and hydro-thermal modelling using experimental data from the literature. Then the validated model is used for modelling of discharge for 2D and 3D cases generated for providing similar conditions to available pilot SWAC system at Brixham laboratory, Brixham, UK.

3. Discharge dispersion modelling

3.1. Micro-scale modelling using OpenFOAM®

To numerically model the discharge dispersion, a solver in the open-source software, OpenFOAM®, was developed. The solver is capable of simulating submerged buoyant water jet discharge into the marine environment under tidal currents and waves. The model is developed for the cases that the submerged jet fluid is water with higher temperature compared to ambient water and the only reason of the buoyancy effect is thermal expansion of the fluid.

The model solves mass, momentum and energy equations for incompressible flow as following,

Mass $$\nabla . u = 0 \quad (1)$$

Momentum $$\rho\left(\frac{\partial}{\partial t}(u) + \nabla.(uu)\right) = -\nabla \mathrm{p} + \nabla.\tau + \rho g \quad (2)$$

Energy $$\frac{\partial T}{\partial t} + \nabla.(uT) = \nabla^2(DT) + \mathrm{S} \quad (3)$$

where u is velocity, ρ is density, t is time, T is temperature, p is pressure, g is the acceleration of gravity, τ is the shear stress tensor and S is a source/sink term. In the solver, the energy and momentum equations are weakly coupled using Boussinesq approximation. This helps to see impacts of the buoyancy effect on the natural convection (buoyancy-driven) dominated flow, $Gr/Re^2 \gg 1$, where Gr is Grashof number and Re is Reynolds number.

Boussinesq approximation is added to the solution considering density as a function of temperature using thermal expansion equation ($\rho \approx \rho_0(1 - \beta(T - T_0))$ in the last term in the right-hand side of the momentum equation (the gravitational term), where β is volumetric temperature expansion coefficient, and ρ_0, T_0 are density and temperature at a reference point, respectively. The model is combined with $k - \omega\ SST$ turbulence closure model to solve turbulent flow. This turbulence model is chosen as it is reliable for modelling of most engineering practical applications.

3.2. Validation

3.2.1. Wave model

The model was validated against different test cases. In this report, a comparison between the results of numerical model against the analytical models in modelling of regular and irregular waves and experimental data of wave flume with a submerged trapezoid bar are provided.

3.2.1.1. Generation and propagation of the regular wave

Based on the regular wave theory, regular waves are sinusoidal with constant wave amplitude (H), wavelength (L) and wave period (τ). Figure 1 shows a well-known diagram by Le Méhauté (2013) which described the validity of different regular wave theories depending on the relative water depth and the wave steepness.

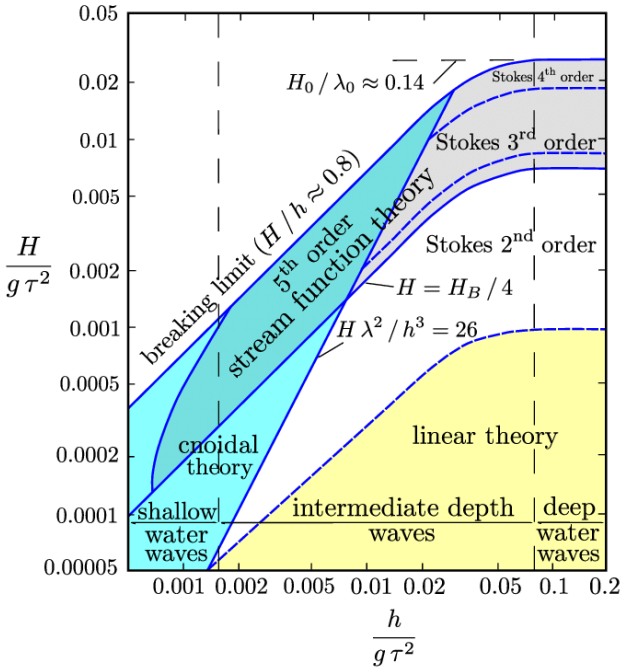

Figure 1. Limits of validity for various wave theories by Le Méhauté (2013).

3.2.1.1.1. Linear wave theory

The linear wave theories, known as Stokes I or Airy wave theory, is the most simple analytical solution for the regular waves which was introduced by Airy (1845). Despite of the easy implementation, Air theory is accurate and practical for wide range of engineering application. In this theory, seawater is assumed to be incompressible and inviscid, and the water motion is irrotational. Other assumptions are that the surface tension is negligible and the pressure at the free surface is constant. The bottom is fixed, and impermeable and wave height is relatively small ($^H/_h \ll 1$). For a two-dimensional Airy wave propagating in x-direction, the free surface displacement and velocity components (u, w) are as the following:

$$\eta(t,x) = \frac{H}{2}\cos(kx - \omega t + \psi) \tag{4}$$

$$u(t,x) = \frac{H}{2}\omega\frac{\cosh(kz)}{\sinh(kh)}\cos(kx - \omega t + \psi) \tag{5}$$

$$w(t,x) = \frac{H}{2}\omega\frac{\sinh(kz)}{\sinh(kh)}\sin(kx - \omega t + \psi) \tag{6}$$

where k is wave number, ω is angular frequency, and ψ is wave phase shift.

angular frequency can be calculated using,

$$\omega = \frac{2\pi}{T} \tag{7}$$

and wave number can be calculated using dispersion relation for water waves,

$$\omega^2 = gk\tanh(kh) \tag{8}$$

where g is acceleration of gravity.

To validate the model for generation of the linear waves, a simulation was run for a wave with specifications provided in Table 1 in a 2D computational domain with 30 m long ad 2 m height. Finer grids were considered for the generated mesh near the free-surface interface, as shown in Figure 2 .

Table 1. linear wave specifications.

Period τ (s)	Wave amplitude H (m)	Water depth h (m)	Wave number k (m^{-1})	Wavelength L (m)
2	0.02	1	1.2039	5.2163

The simulation was run for 30 s and results in terms of time evolution of the surface elevation of propagating were compared with analytical solution in 4 different distances from the inlet of the computational domain (e.g. $x = 0.5L,\ 1L,\ 2L,\ 3L$). The results are provided in Figure 3 and show good agreement between CFD and analytical results.

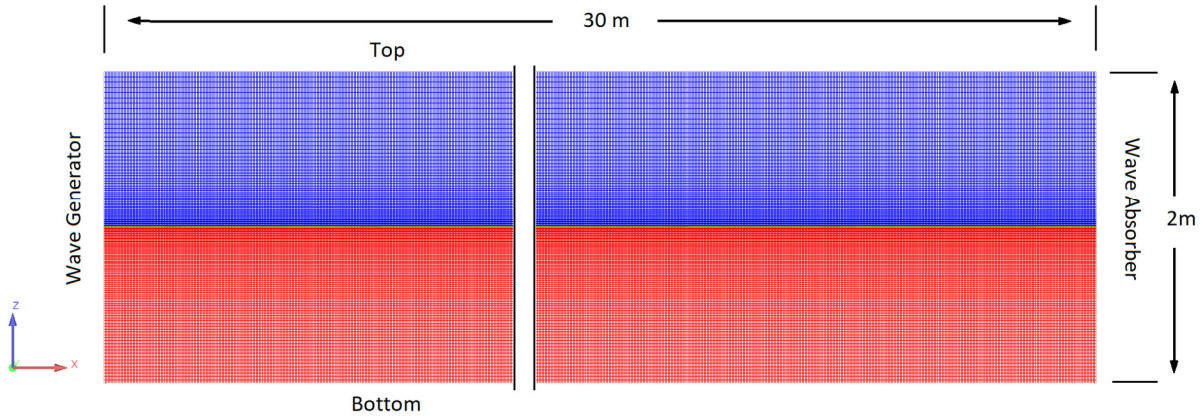

Figure 2. Generated mesh for linear wave simulation.

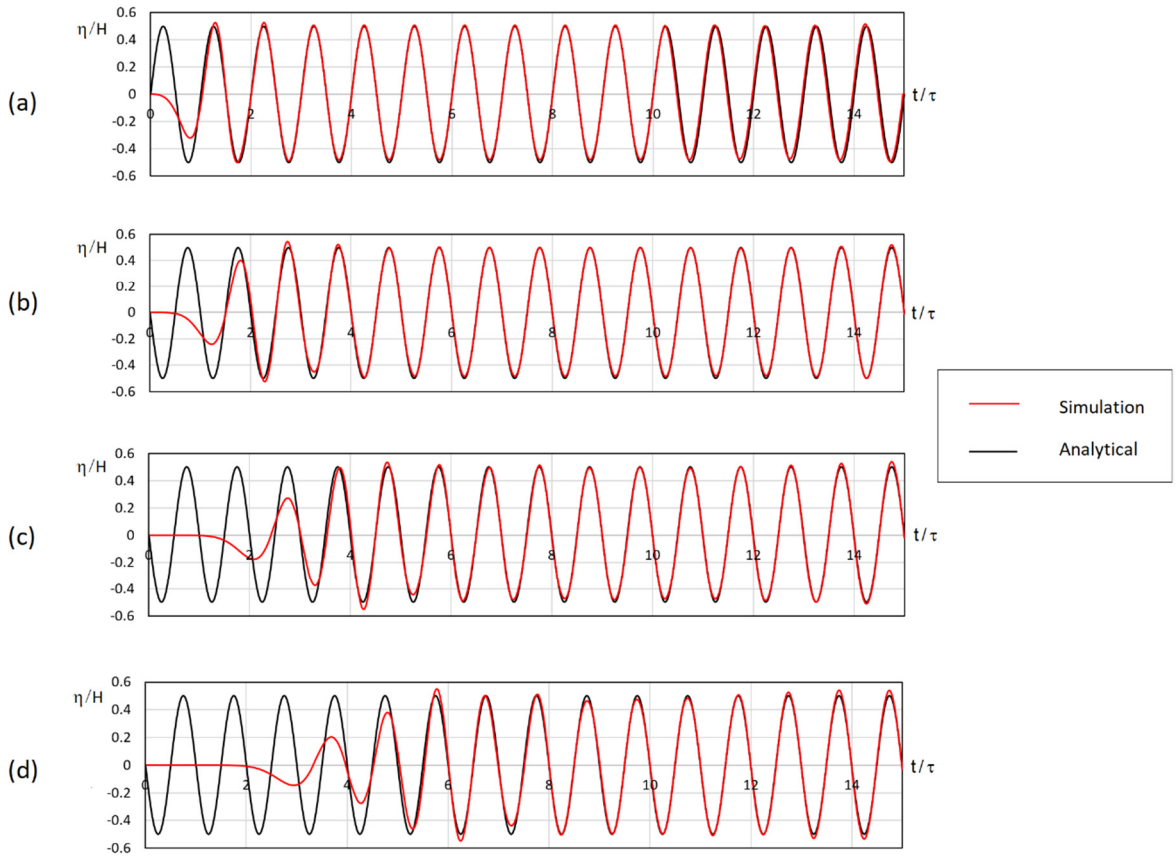

Figure 3. Analytical solution and simulation results for the linear wave, (a) x=0.5L, (b) x=L, (c) x=2L, (d) x=3L.

3.2.1.1.2. Non-linear Stokes II wave theory

Stokes in 1847 for the first time established the nonlinear solution using the perturbation theory for the regular waves, known as Stokes expansion. Based on the Stokes expansion, the relevant equations for the Stokes II wave surface displacement and velocity components are described by adding the second order (quadratic) term to linear wave theory as follows, respectively,

$$\eta(t,x) = \frac{H}{2}\cos(\theta) + k\frac{H^2}{4}\frac{3-\tanh^2(kh)}{4\tanh^3(kh)}\cos(2\theta) \quad (9)$$

$$u(t,x) = \frac{H}{2}\omega\frac{\cosh(kz)}{\sinh(kh)}\cos(\theta) + \frac{3}{4}\frac{H^2\omega k\cosh(2kz)}{4\sinh^4(kh)}\cos(2\theta) \quad (10)$$

$$w(t,x) = \frac{H}{2}\omega\frac{\sinh(kz)}{\sinh(kh)}\sin(\theta) + \frac{3}{4}\frac{H^2\omega k\sinh(2kz)}{4\sinh^4(kh)}\sin(2\theta) \quad (11)$$

To validate the model for generation of a non-linear Stokes II wave theory, a wave with the provided specifications at Table 2 was defined.

Table 2. Non-linear wave specifications.

Period τ (s)	Wave amplitude H (m)	Water depth h (m)	Wave number k (m^{-1})	Wavelength L (m)
2.2	0.04	0.4	1.5259	4.1156

For this test case, a 2D rectangular computational domain with 30 m long and 1 m height was generated, and finer grid cells were considered near the free-surface interface area. A mesh dependency study was done and a mesh with around 270,000 grid cells with the smallest cells size of 0.01 m × 0.005 m was chosen for the simulations. The simulation results for the first 22 s of the simulation for the surface elevation were compared with analytical solution at 4 different distances from the inlet (i.e. $x = 0.5L,\ 1L,\ 2L,\ 3L$), as shown in Figure 4. Similar to simulations for linear wave, good agreement between CFD and analytical results were observed, while with progress in time and distance from the wave generator boundary a small deflection from the analytical solution could be seen.

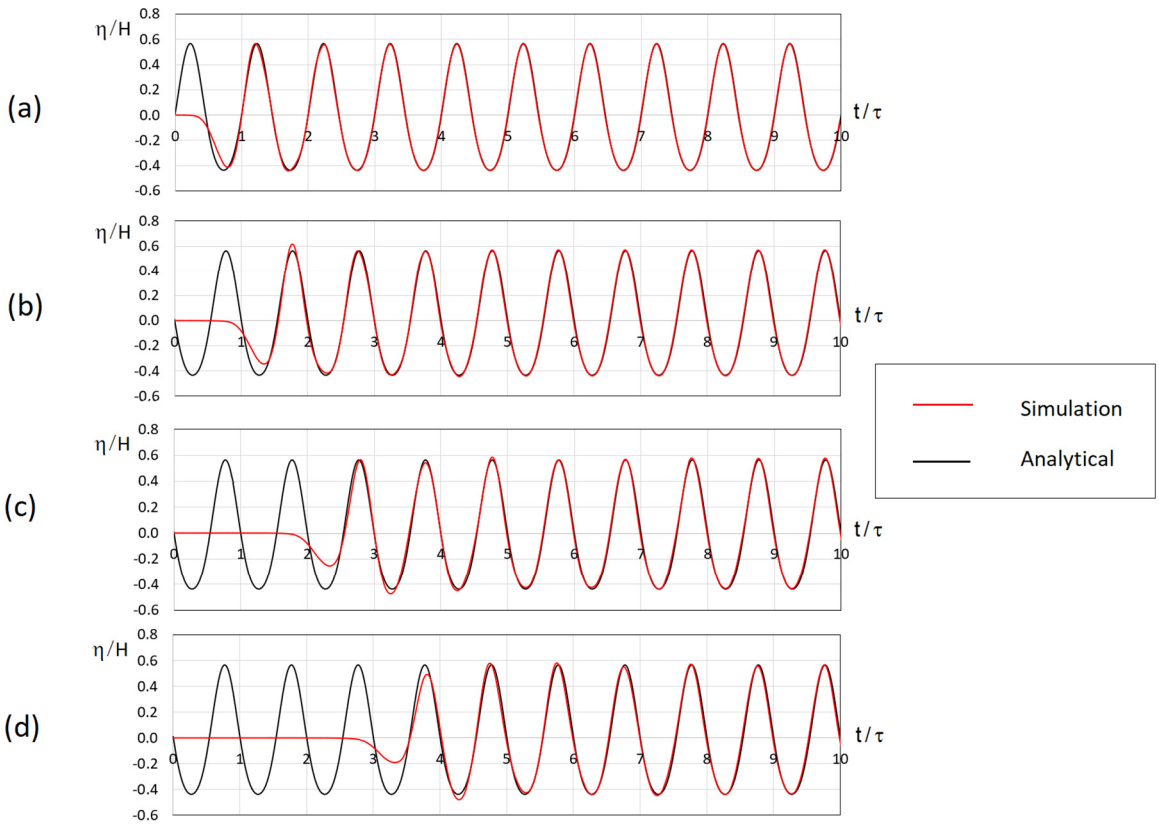

Figure 4. Analytical solution and simulation results for the non-linear wave, (a) x=0.5L, (b) x=L, (c) x=2L, (d) x=3L.

3.2.1.2. Generation and propagation of the irregular wave

An irregular wave is constructed by linear superposition of regular wave components. Hence, for the purpose of the validation of the CFD model for an irregular wave, generation of an irregular wave,

using linear superposition of a group four regular linear waves as listed in Table 3 with different wave phase shift was considered, as presented in Figure 5a.

A same computational domain of the regular linear wave test was considered. The simulation results of wave surface elevation at $x = 3\ m$ away from the inlet can be seen in Figure 5b. The results prove the high capability of the CFD model in simulation of the irregular waves.

Table 3.Specifications for linear waves to generate the irregular wave.

Waves	Period τ (s)	Wave amplitude H (m)	Water depth L (m)	Wave number k (m^{-1})
No.1	1.8	0.02	1	1.4011
No.2	0.95	0.008	1	4.4557
No.3	1.3	0.01	1	2.417
No.4	2.5	0.03	1	0.8988

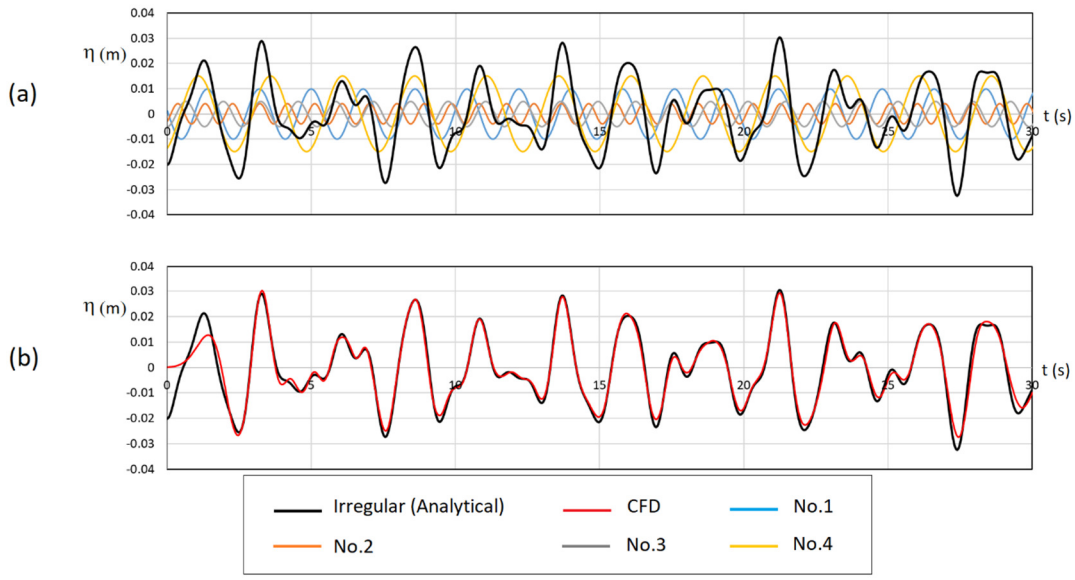

Figure 5.(a) linear waves to generate the irregular wave, (b) Analytical solution and simulation results for the irregular wave at x= 3(m).

3.2.1.3. wave flume with a submerged trapezoidal bar

The model was also validated against the experimental data by Beji and Battjes (1994) for interaction of the regular wave with a submerged breakwater. Beji and Battjes (1993, 1994) conducted a series of experimental tests in a wave flume with a submerged trapezoid bar for regular and irregular waves. The test was conducted in a flume with 37.7 m long, 0.8 wide, and 0.75 m deep. The entire set of experiments were done with a still water level of 0.4 m. The toe of the trapezoid bar was located at 6 m from the wave-generation board, while a beach with a 1:25 slope was presented at the other end of the flume to serve as a wave absorber. More detail of the experiment can be found in (Beji and Battjes, 1993). In Beji and Battjes (1994), one of the tests was run with periodic incident nonbreaking waves with period of $T = 2\ s$ and wave height of $H = 0.02\ m$. As a result of the experiment, surface

elevations changes at 6 different stations above and downstream of the breakwater for 10 s of the test were reported.

To reproduce the result using the developed numerical model, a numerical setup for the test included a two-dimensional computational domain 21 m long and 1 m high as shown in Figure 6 were made. The numerical setup is similar to experimental flume, whereas the breakwater toe was placed at 2 m from the wave generator boundary and the beach at the end of the flume is replaced with a wave absorption boundary. A cell stretching wave damping technique as suggested by Mohseni and Soares (2022) was also considered to ensure suppressing wave reflections. A second-order regular wave was generated at the wave generator boundary and propagated toward the trapezoid-bar. An initial mesh dependency study was carried out for the numerical setup for meshes with different size as given in Table 4 and the coarse mesh was chosen for the rest of the simulations. The smaller grid size was considered near the free-surface region along the whole domain in each case. Simulations with were carried out for 40 s. A comparison between the simulation results for the last 10 s of the simulations and the laboratory measurement results by Beji and Battjes (1994) is provided in Figure 7. Overall, a good agreement can be seen between the results in all stations in terms of generation of the crest and trough.

Table 4.

Mesh	Number of Grids (millions)	Smallest grid size (cm)
Coarse	0.35	0.5 × 0.13
Medium	0.55	0.25 × 0.13
Fine	0.7	0.25 × 0.06

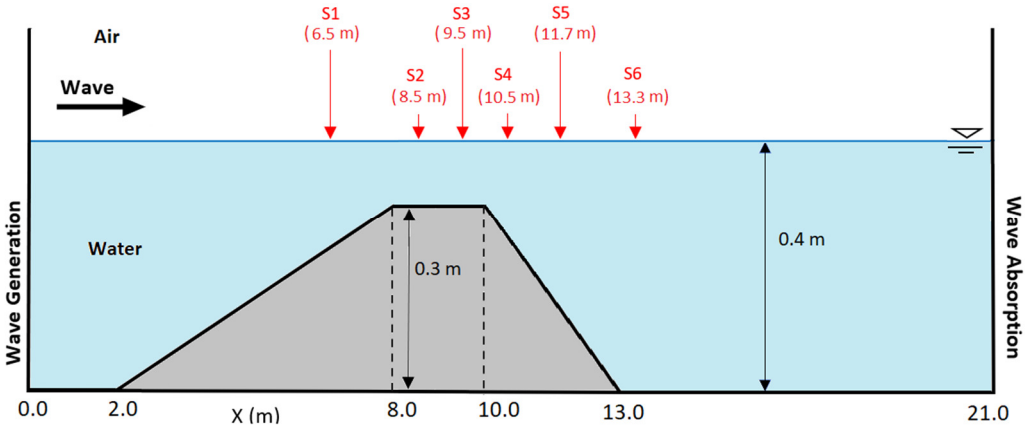

Figure 6. Schematic of the generated mesh for wave flume with a trapezoid bar test.

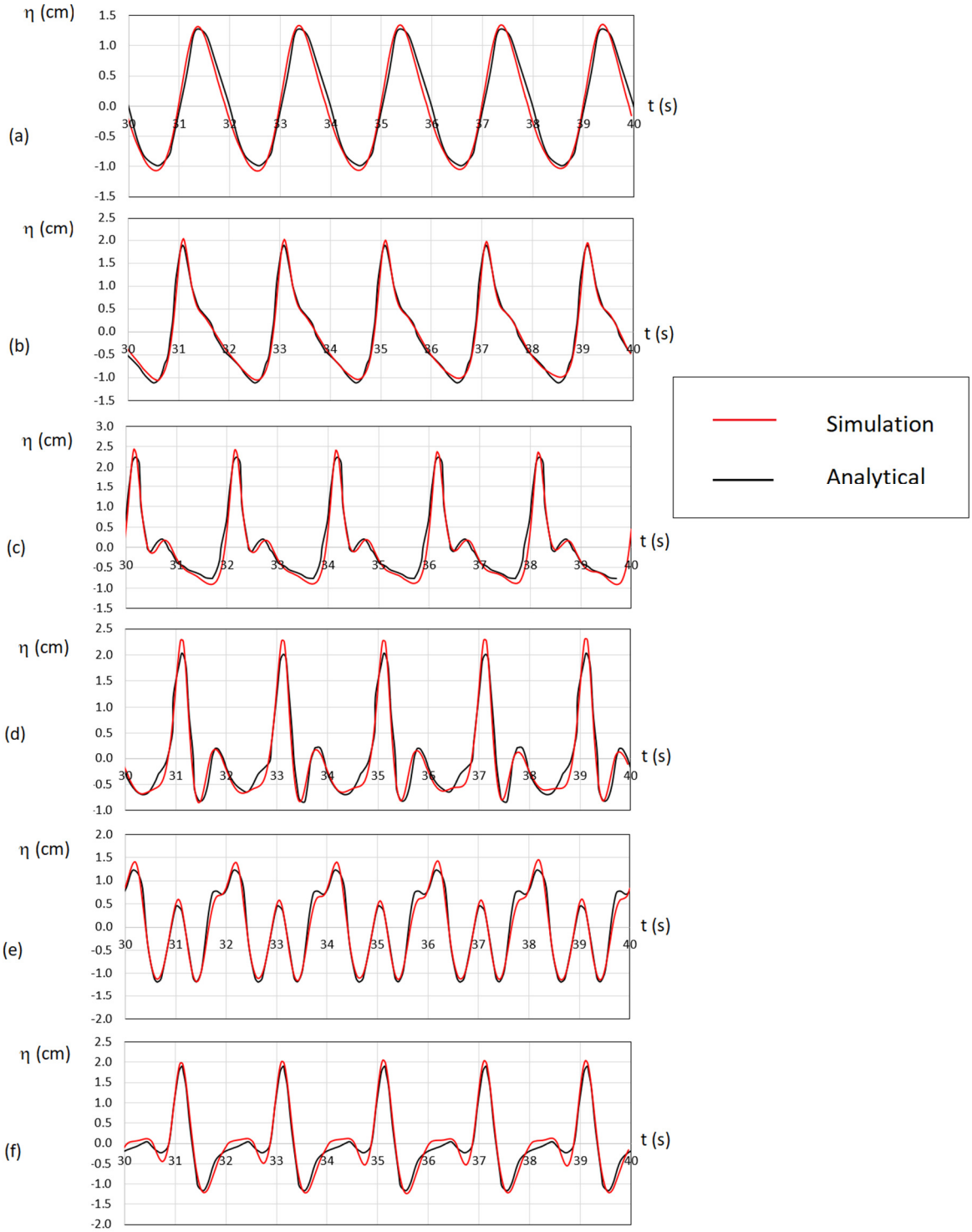

Figure 7. Experimental and simulation results for wave flume with a trapezoid bar test (a) sensor1, (b) Sensor2, (c) Sensor3, (d) Sensor4, (e) Sensor5, (f) Sensor6.

3.2.2. Hydro-Thermal Model

To validate the hydro-thermal part of the model, experimental data conducted by Sobey et al. (1989) for horizontal round buoyant jet in stagnant shallow water was considered. The experiment was carried out in a 3 m × 3 m square by 0.35 m deep tank. The water jet inlet diameter, D_0, was 27.5 mm. A horizontal hot water jet inlet was placed at the horizontal centreline at one end of the tank (see Figure 8). The buoyancy parameter was held constant at nominally 0.003 for all the tests. In total, 75 tests were carried out for different water depth and different jet depth and speed. The results were categorized into 4 groups based on the range of free surface parameters, $(H - Z_0)/l_M$, where l_M is length scale, where Sobey et al. (1989) suggested to be calculated using,

$$l_M = \left(\frac{\pi}{4}\right)^{0.25} D_0\, Fr \qquad (12)$$

where Fr is Froude number. As a results of the experimental study, Sobey et al. (1989) provided the data regarding the centreline path of the jet for the tests in each category. Two tests from each category were simulated (Table 5) and compared with the experimental results for model validation as shown in Figure 9. Promising agreement between the experimental and simulation results were observed. A small difference between the results can be noticed in Figure 9 for categories 1 and 2, while this difference is negligible considering the z-axis label values. These results prove that the implemented hydro-thermal model is capable of modelling of discharge dispersion for a case of a SWAC system.

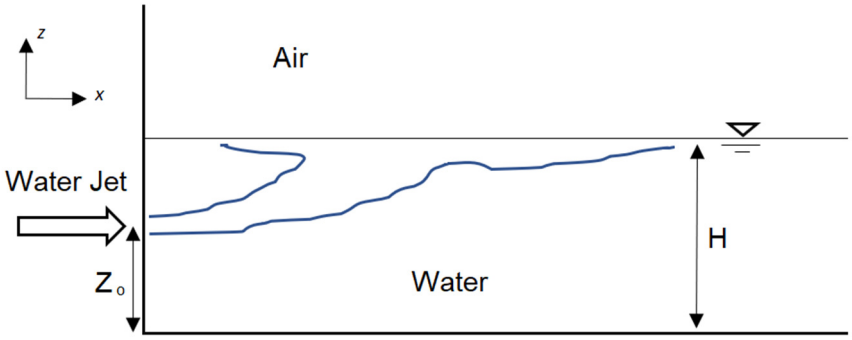

Figure 8. schematic of the test by Sobey et al. (1989).

Table 5. chosen test for hydro-thermal modelling.

Categories	Categories No.	Number of tests in the category	Sim. Test number	$H\,(m)$	$Z_0(m)$	$l_M(m)$	Flow rate (l/s)
$0.075 \le (H - Z_0)/l_M \le 0.1$	1	5	58	0.1	0.075	0.266	0.173
			59	0.1	0.075	0.327	0.212
$0.125 \le (H - Z_0)/l_M \le 0.15$	2	3	57	0.1	0.075	0.191	0.125
			65	0.1	0.05	0.393	0.254
$0.3 \le (H - Z_0)/l_M \le 0.4$	3	8	45	0.2	0.05	0.382	0.252
			61	0.1	0.05	0.135	0.088
$0.5 \le (H - Z_0)/l_M \le 1.0$	4	16	36	0.2	0.1	0.128	0.083
			43	0.2	0.05	0.254	0.170

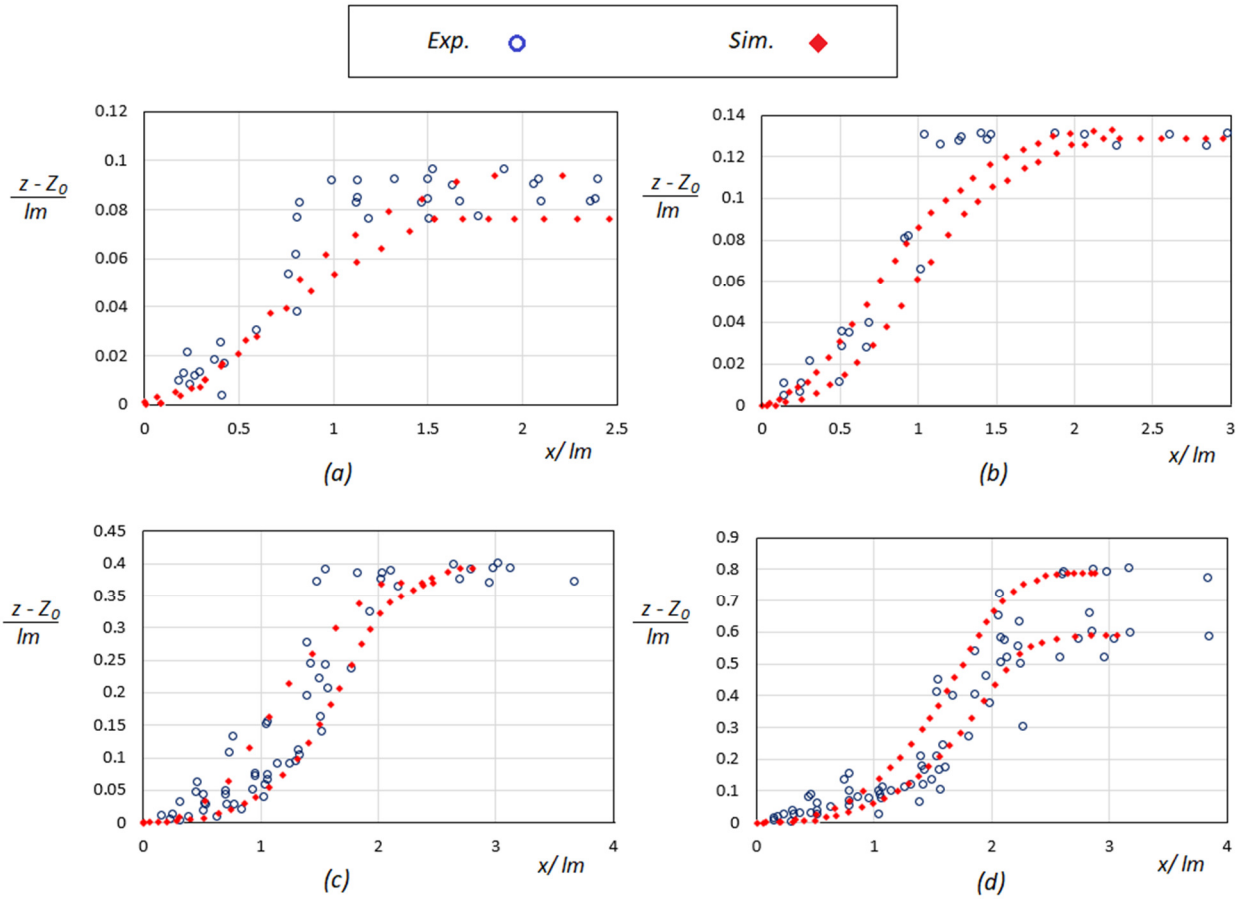

Figure 9.Experimental and Simulation results for hydro-thermal test case by Sobey et al. (1989) for different categories, (a) No.1, (b) No.2, (c) No.3, (d) No.4.

3.3. Simulations

3.3.1. 2D test cases with a discharge dispersion for different water level

In this test case, there is no wave or current flow in the domain and the water is stagnant. An inlet of a warm water, $T = 320\ K$, from the right side of the domain, coastal side, is discharged to the domain with ambient temperature of $T = 300\ K$.

Three different water level was considered for this test case to hot water discharge interactions with low-, mid-, and high-tide conditions (See Figure 10). For each case, the computational domain roughly includes 10000 grids, with finer cell size near the interface and discharge area (See Figure 11).

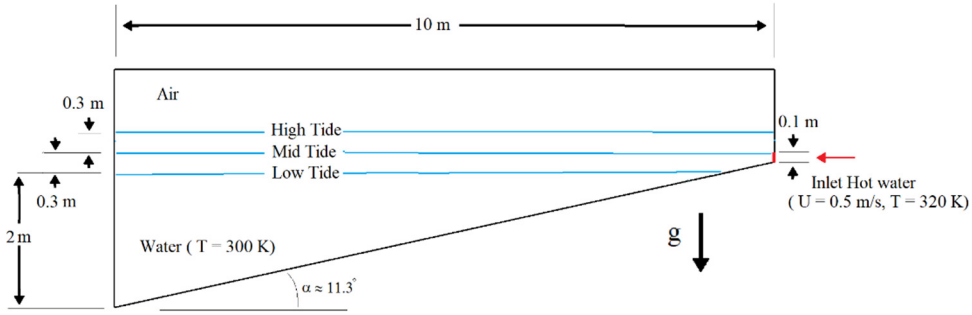

Figure 10. Schematic of the domain for 3 different water levels.

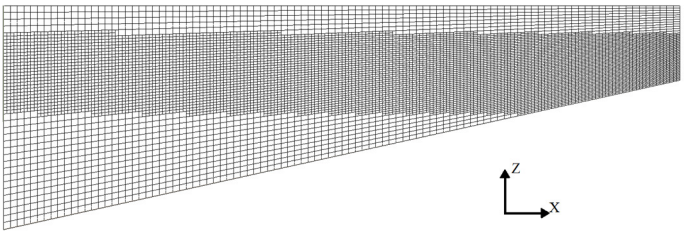

Figure 11. Computational domain for the case of mid-tide water level.

The temperature distribution results after 40 and 80 s of the simulation is provided in Figure 12, Figure 13, and Figure 14 for low-, mid-, and high-water level tide cases, respectively. The simulation result shows that in all cases, initially the warm water inlet flow tends to be attached to the adjacent bed surface and resist to merge, a phenomenon called Coanda effect. After this stage, when the fluid movement is dominated by buoyancy effect due to the density difference between the warm water and cold ambient water, the warm water flow moves upward and reach the free-surface or water/air interface. The simulation results reveal that the buoyancy effect keeps the warm water from mixing with the ambient water, and therefore, the warm water will be spread over the free surface. These results illustrates that even an small temperature difference between the warm discharge water and the ambient cold water, in this case 20 K, can make a noticeable impacts on mixing behaviour of the discharge water.

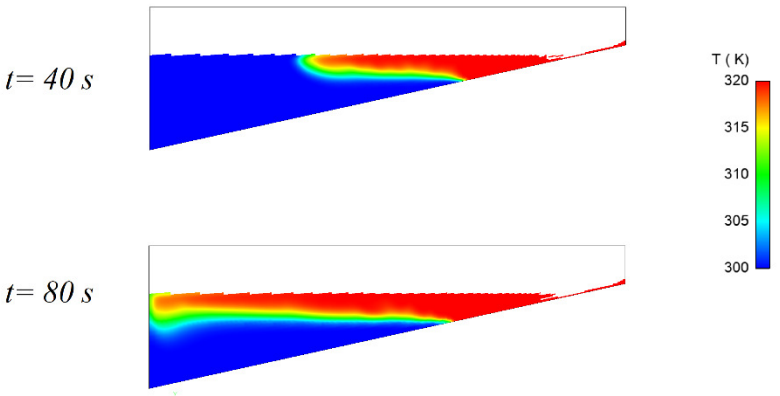

Figure 12. Simulations for low-tide case.

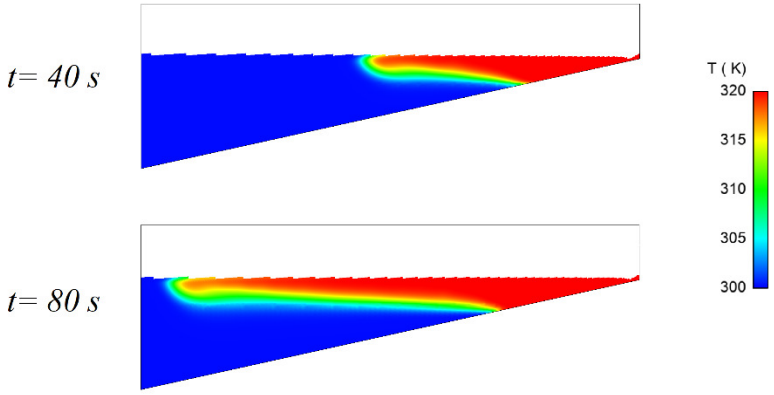

Figure 13. Simulations for mid-tide case.

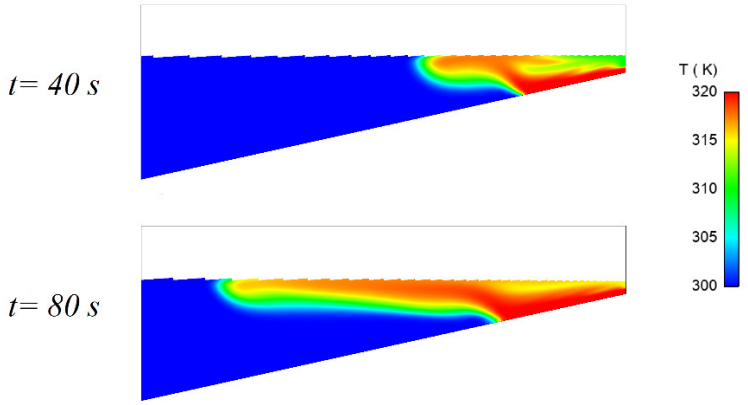

Figure 14. Simulations for high-tide case.

3.3.2. 3D test case of discharge dispersion for different current velocity speed

In this test cases, a condition very close to the discharge water from pilot SWAC system at Brixham laboratory to Brixham harbour is modelled. Figure shows the location of the intake and discharge pipelines at the Brixham harbour. The discharge pipeline is located at the coastline. Due to very small value of the discharge water (roughly flow rate of 100- 200 lit/min) a 20 m × 20 m geometry was considered (red dashed-line in Figure 15). Figure 16 shows the assumed condition for the simulations. A discharge of warm water, $T = 310\ K$, from the coastal side of the geometry, into a 3D domain with ambient temperature of $T = 300\ K$ is simulated. Due to the presence of the breakwater at Brixham harbour, the impacts from waves are neglected. Therefore, the simulations were run only under current due to the tidal flow. Three different current velocities, $U_{current} = 0.1, 0.05, 0.01\ m/s$, were investigated which were chosen based on the maximum and minimum current velocity at the Brixham harbour from Copernicus data. The geometry of the bed slope was estimated based on the available Brixham harbour bathymetry data. The discharge inlet to the domain is considered at 5 m away from the inlet of the current flow.

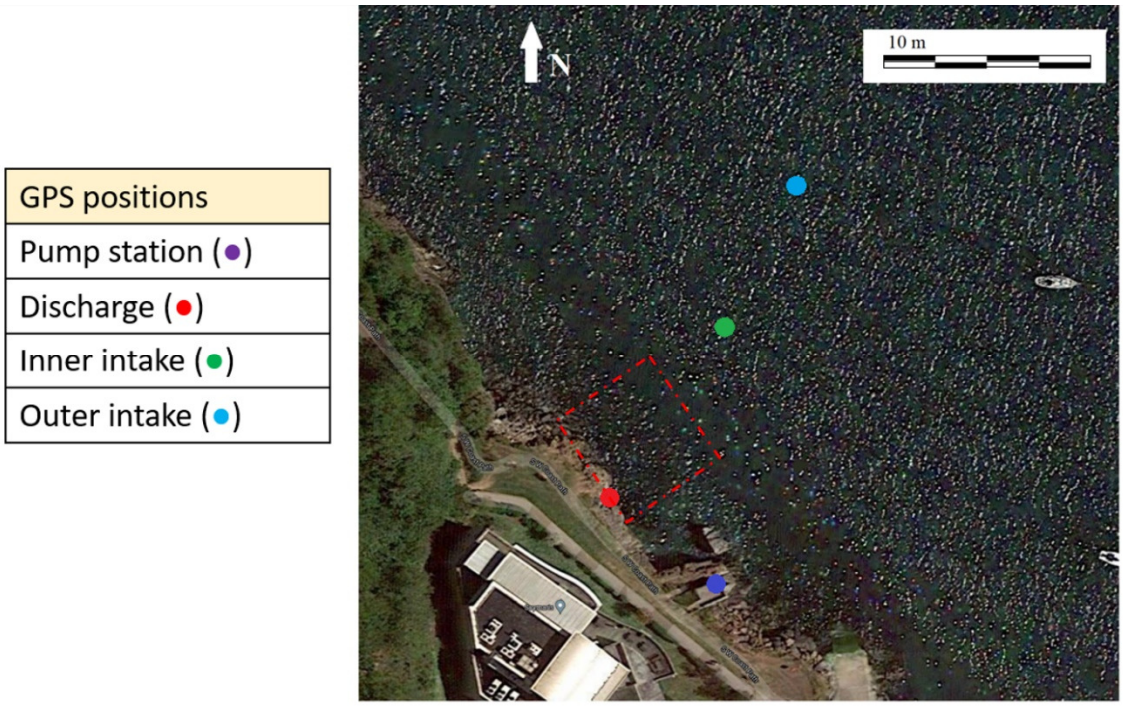

Figure 15. considered domain for 3D test case of discharge dispersion based on Brixham site.

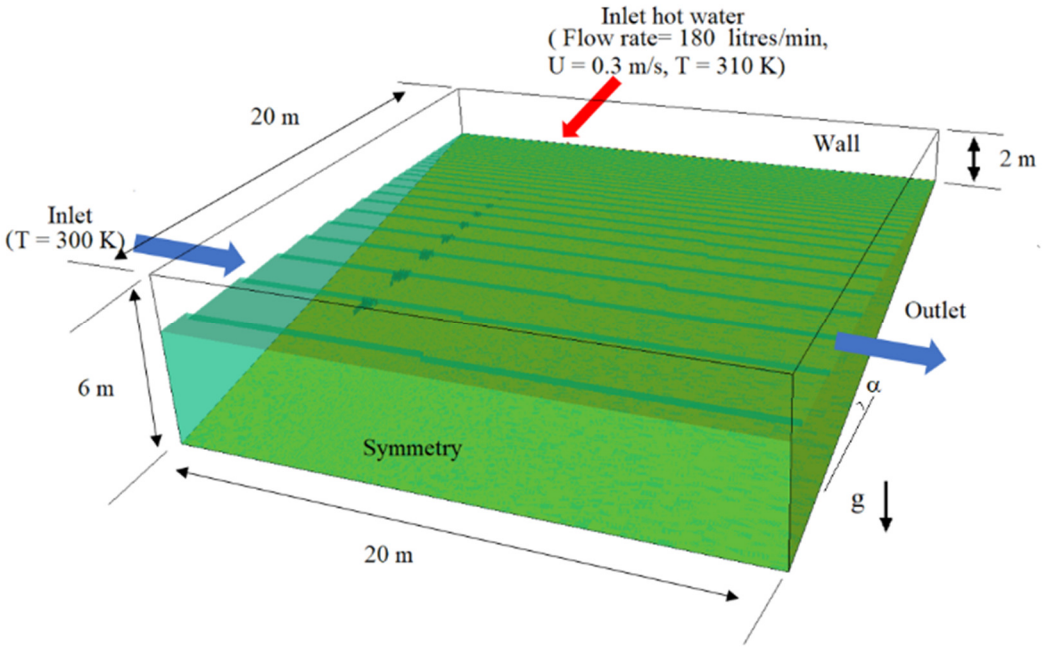

Figure 16. generated domain for 3D test case of discharge dispersion based on Brixham site.

A computational domain with around 1.2 million cell grids with finer mesh near the discharge area were generated. Each simulation was run for t = 100 s. The simulation result at the t = 100 s is presented in Figure 17. In Figure 17, the bed boundary of the computational domain is shown in green, the water/air interface is presented in light blue. To track the dispersion of the warm water plume, an iso-surface technique for T= 301 K is applied, which is displayed in orange. In the results, the plume dispersion is clearly dominated by direction and the magnitude of the current flow. Increase in the current speed increase the plume propagation length toward the direction of the current flow. On the other hand, it was realized that almost in all cases, the warm water plume was attached to the bottom surface of the domain due to Coanda effect while this impact is stronger in higher current flow speed. This can be due to small temperature difference between the warm water discharge and the ambient water and the impact of the higher speed current flow that led to faster mixture of the discharge with ambient water.

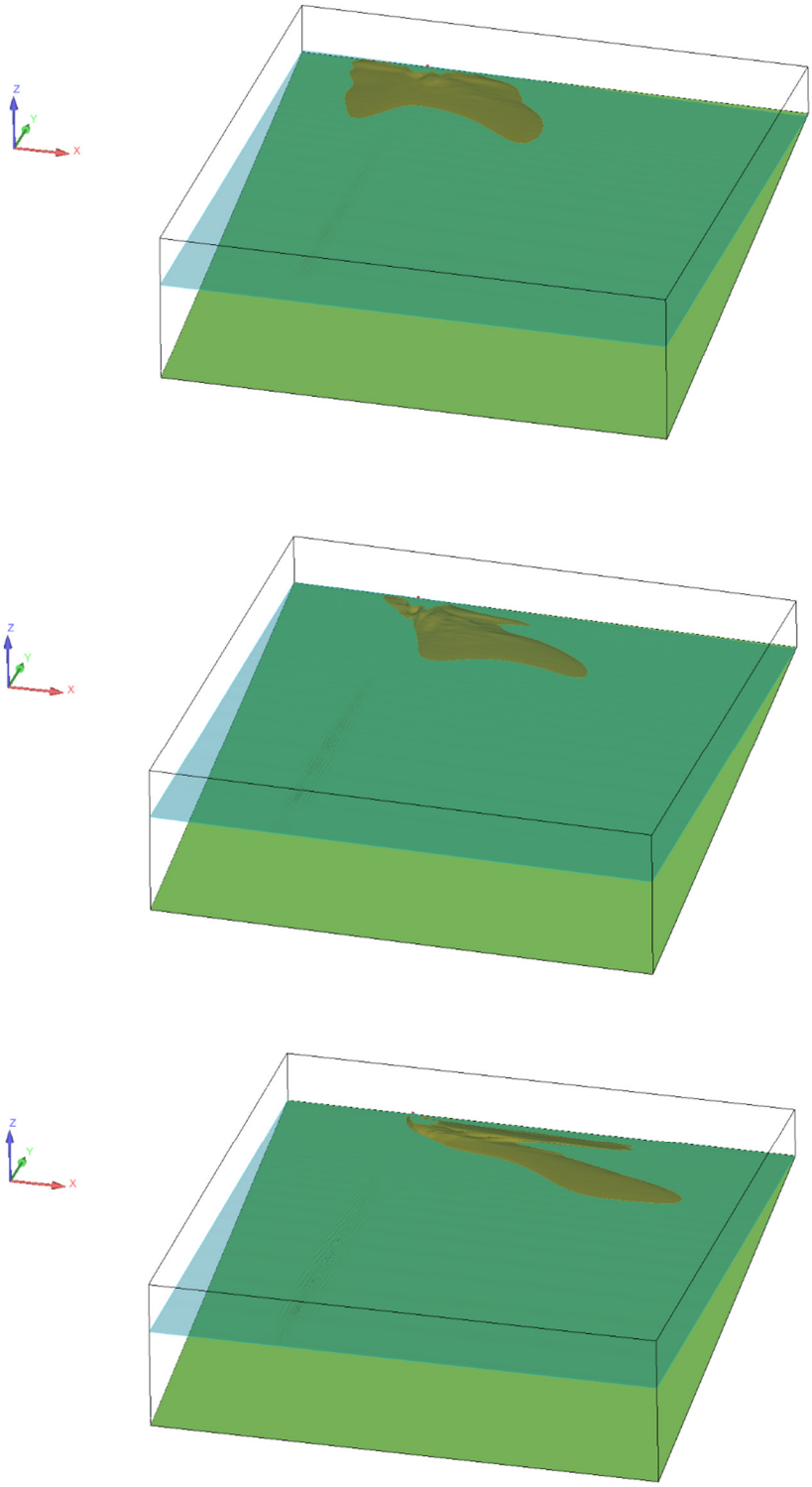

Figure 17. Simulation results for 3D test case of discharge dispersion based on Brixham site.

4. References

AIRY, G. B. 1845. *Tides and waves*, B. Fellowes.

LE MÉHAUTÉ, B. 2013. *An introduction to hydrodynamics and water waves*, Springer Science & Business Media.